Upwelling source depth in the presence of nearshore wind stress curl

M. G. Jacox[1] and C. A. Edwards[1]

Received 27 December 2011; revised 16 March 2012; accepted 17 March 2012; published 5 May 2012.

[1] The influence of nearshore wind stress curl on the relative partitioning of bottom boundary layer (BBL) and interior transport within an idealized, two-dimensional coastal upwelling system is studied theoretically and using a numerical model. A nearshore reduction in upwelling favorable wind stress amplitude (1) reduces the width of the inner shelf, (2) reduces the local wind-driven Ekman transport, and (3) increases the cross-shelf momentum flux divergence. Relative BBL transport, defined as the transport entering the surface mixed layer (SML) from the BBL divided by offshore transport in the SML, decreases under reduced nearshore wind stress. This effect is dominated by the reduced local SML Ekman transport and to a lesser degree by local curl of surface and bottom stresses. We consider the quantitative impact for a range of shelf slopes, stratifications, and wind stress curl scales. The relative contribution of bottom boundary layer transport co-varies with upwelling source depth and is therefore expected to alter nutrient fluxes into the euphotic zone as well as the resultant biological response.

Citation: Jacox, M. G., and C. A. Edwards (2012), Upwelling source depth in the presence of nearshore wind stress curl, *J. Geophys. Res.*, *117*, C05008, doi:10.1029/2011JC007856.

1. Introduction

[2] Wind-driven upwelling of nutrient-rich subsurface water in eastern boundary currents (EBCs) may be forced by two mechanisms; coastal divergence in the surface layer due to equatorward winds at the coast, and Ekman pumping driven by cyclonic wind stress curl. The coastal divergence component (also referred to simply as coastal upwelling in this paper) occurs in a relatively narrow band next to the coast, resulting in strong vertical velocities nearshore. Ekman pumping (also referred to as curl-driven upwelling) may extend far offshore, driving lower upwelling velocities over a much larger area (up to 200–300 km in the California Current System (CCS) [*Pickett and Paduan*, 2003]). In the nearshore region of strong coastal upwelling, Ekman pumping is generally thought to be of little importance except in the vicinity of significant coastal promontories, where wind stress curl may produce upwelling rates on the same order as those due to alongshore winds [*Koracin et al.*, 2004]. Offshore of the narrow coastal band, weaker curl-driven upwelling dominates and vertical transport driven by the two components are of the same order when integrated over the entire upwelling region [*Enriquez and Friehe*, 1995; *Pickett and Paduan*, 2003; *Rykaczewski and Checkley*, 2008].

[3] Several studies have addressed the influence of nearshore curl not only on upwelling transport, but also on source waters and nutrient flux. In observations off Bodega Bay, CA, *Dever et al.* [2006] estimated curl-driven vertical nitrate flux divergence to be about half that due to alongshore winds at the coastal boundary, and total nitrate flux integrated over the area of positive curl to be several times higher than that from coastal upwelling. *Capet et al.* [2004] studied the upwelling response to two wind profiles in a realistic model off Central California; one with a much stronger nearshore drop-off in wind stress. They tracked vertical displacement of Lagrangian tracers in each case, and found that upwelling in the upper 100 m is primarily associated with intense, localized coastal upwelling, not vertically and horizontally distributed Ekman pumping. *Messié et al.* [2009] calculated nitrate fluxes in all four major EBCs from QuikSCAT winds and in-situ nitrate profiles, and estimated the curl-driven contribution to upwelled nitrate at just 21.5–31.4%. Conversely, in models of the Peru and California coasts, respectively, *Albert et al.* [2010] and *Song et al.* [2011] conclude that reduced equatorward winds nearshore (cyclonic wind stress curl) cause a shoaling of the nutrient-rich poleward undercurrent, increasing nutrient flux overall.

[4] Surface winds are routinely measured from a number of platforms, each valuable but with limitations. In situ measurements from moorings and aircraft are the most accurate, but data are sparse. Satellites offer much improved coverage, but data inshore of 25–50 km from the coast are unreliable and nearshore wind profiles are highly dependent on the satellite product used [*Croquette et al.*, 2007]. In modeled winds, the coastal curl band typically becomes stronger and narrower as resolution increases, and wind profiles do not necessarily converge at high resolution

[1]Department of Ocean Sciences, University of California, Santa Cruz, California, USA.

Corresponding Author: M. G. Jacox, Department of Ocean Science, University of California, 1156 High St., Santa Cruz, CA 95062, USA. (mjacox@ucsc.edu)

0148-0227/12/2011JC007856

Table 1. Parameters for Numerical Model Runs[a]

Run	α (10^{-3})	N (10^{-3} s^{-1})	S	ϵ (km)
1	2	4	0.08	0
2	2	12	0.24	0
3	2	20	0.40	0
4	6	4	0.24	0
5	6	12	0.72	0
6	6	20	1.2	0
7	10	4	0.40	0
8	10	12	1.2	0
9	10	20	2.0	0
10–18	2–10	4–20	0.08–2.0	10
19–27	2–10	4–20	0.08–2.0	20
28–36	2–10	4–20	0.08–2.0	40

[a]A total of 36 runs are represented to cover widely ranging shelf slope (α), stratification (N), and cross-shelf scale of wind stress curl (ϵ, as described by equation (2)). Runs 10–18, 19–27, and 28–36 are repeats of 1–9, except for changes in ϵ.

[*Capet et al.*, 2004]. Consequently, considerable uncertainty remains in the nearshore wind structure, and its variability in space and time.

[5] *Lentz and Chapman* [2004] demonstrated the dependence of cross-shelf transport structure on a topographic Burger number,

$$S = \frac{\alpha N}{|f|}. \tag{1}$$

The Burger number is dependent on the slope of the continental shelf, α, the buoyancy frequency, $N = \sqrt{(-g/\rho_0)\partial\rho/\partial z}$, where ρ is the fluid density, ρ_0 is a reference density and g is gravitational acceleration, and the Coriolis frequency, $f = 2\Omega\sin\phi$, where $\Omega = 7.29 \times 10^{-5}$ s^{-1} is Earth's rotation rate and ϕ is latitude. Low Burger numbers produce onshore flow concentrated in the bottom boundary layer (BBL), while increased Burger number shifts onshore flow to the interior. *Jacox and Edwards* [2011] investigated the influence of individual Burger number parameters on nutrient fluxes and source depth during upwelling and found results to be more complex than those for physical transport alone. The greatest source depths reached were in a weakly stratified water column with steeply sloping shelf. In both studies, however, only spatially uniform wind-forcing was considered. Here we use a simple idealized model, not specific to any particular region, to investigate the sensitivities of upwelling transport and source depth to changes in Burger number, two of its individual components (topography and stratification), and the structure of nearshore wind stress.

2. Methodology

[6] We use the Regional Ocean Modeling System (ROMS) [*Shchepetkin and McWilliams*, 2005] in a two-dimensional configuration (two alongshore grid points). Topographic bottom slope and initial stratification are spatially uniform for each model run and are varied between runs as outlined in Table 1. Further details of the model are presented in *Jacox and Edwards* [2011], which also notes several important model omissions such as a shelf break and an alongshore pressure gradient. The model configuration represents an oceanic eastern boundary and is illustrated schematically in Figure 1; here y is directed northward, x is directed eastward with $x = 0$ at the coastal boundary ($x < 0$ within the domain), and z is directed upward with the unperturbed ocean surface at z = 0. The ocean bottom is at depth $h = h_o - \alpha x$, where the coastal bottom depth h_o is assumed to be zero for purposes of the theory in section 3. It is convenient for clarity of presentation to place the system in the northern hemisphere with $f > 0$ and have negative surface stress ($\tau^{sy} < 0$) imply upwelling favorable conditions, though the derivation for $f < 0$ is straightforward and the discussion is general. For budgeting purposes, the model domain is divided into surface and bottom mixed layers, an interior, and the inner shelf where boundary layers converge. Bottom boundary layer (U^b) and surface mixed layer (U^s) transports are assumed equal to their Ekman transports, and the overall interior transport (U^i) is defined such that no net cross-shelf transport occurs for any x: $U^i = -(U^s + U^b)$. In the usual configuration of upwelling favorable wind stress considered here, U^s is negative, whereas U^b and U^i are positive.

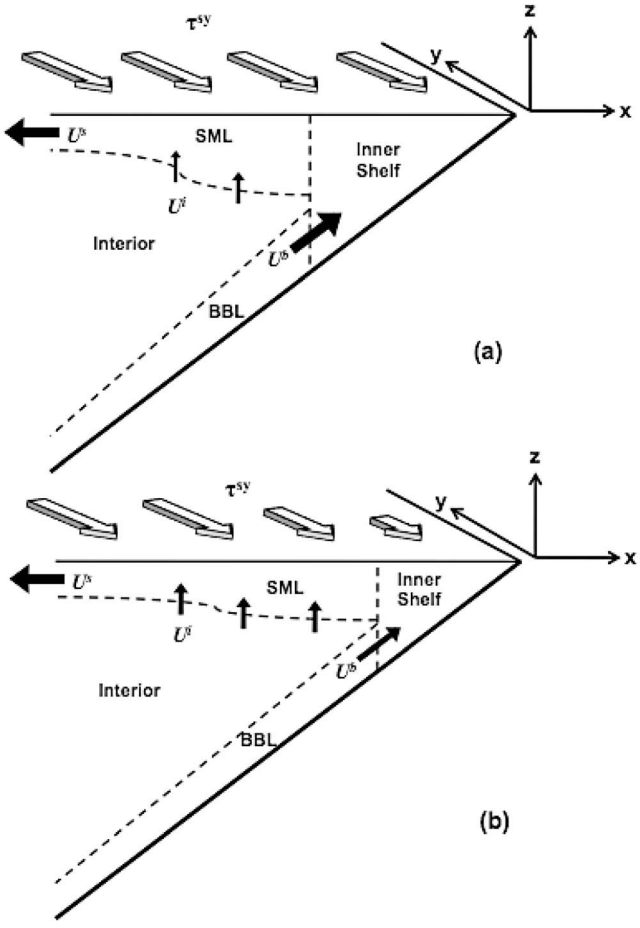

Figure 1. Schematic of model configuration and transport budget for (a) uniform winds and (b) a nearshore wind stress reduction (positive curl). The domain is divided into four regions: the surface mixed layer (SML), bottom boundary layer (BBL), interior, and inner shelf. Black arrows indicate BBL (U^b), interior (U^i), and surface (U^s) components of upwelling transport. The nearshore wind stress reduction produces a smaller inner shelf and shifts upwelling transport from the BBL to the interior. Transport far offshore in the SML is the same in both cases.

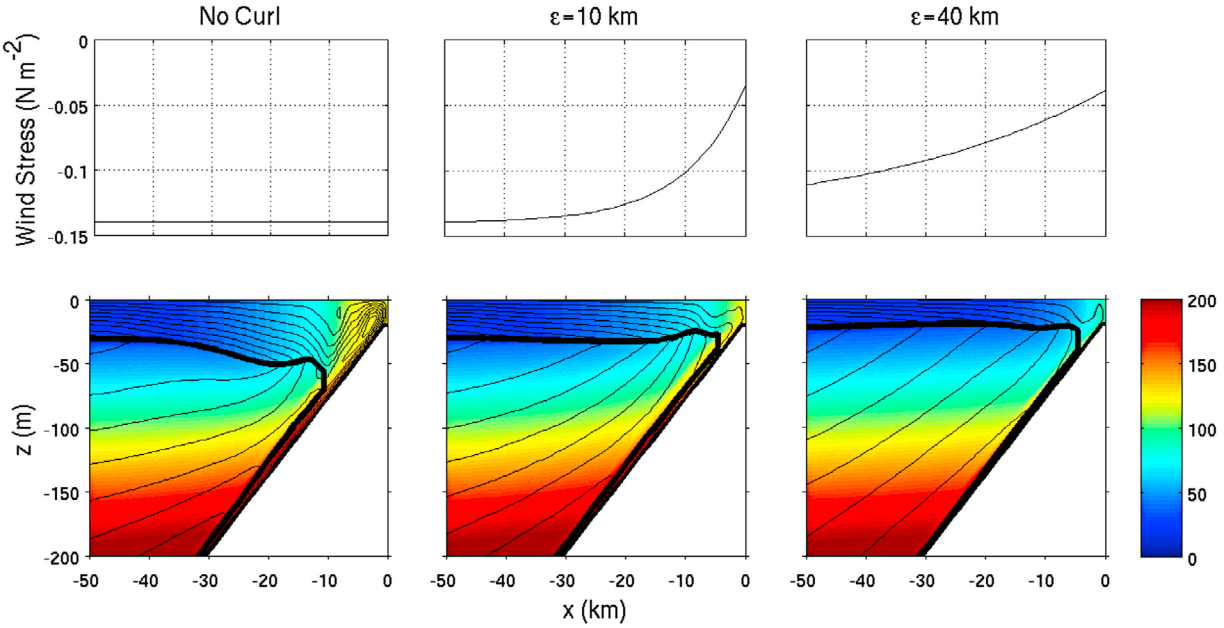

Figure 2. Upwelling response after 10 days is depicted under 3 wind patterns, for model simulations with $\alpha = 0.006$ and $N = 0.012\ s^{-1}$ (from left to right, runs 5, 14, and 32 in Table 1). (top) Cross-shelf structure of equator-ward wind stress; (bottom) streamlines (thin black lines) overlaid on "source depth tracer" concentration (color). The surface mixed layer, bottom boundary layer, and offshore extent of the inner shelf are marked by thick black lines.

[7] We represent the cross-shelf wind profile with an analytical function of the form

$$\tau^{sy} = \tau_c + (\tau_o - \tau_c)\left(1 - e^{x/\epsilon}\right), \tag{2}$$

where $\tau_c = -0.04\ \mathrm{Nm}^{-2}$ is the coastal wind stress, $\tau_o = -0.14\ \mathrm{Nm}^{-2}$ is the offshore value, and ϵ is the cross-shelf e-folding distance for wind stress. Model wind profiles are shown in Figure 2. In addition to curl-free runs ($\epsilon = 0$ km) we perform runs with $\epsilon = 10$, 20, and 40 km, where 90% of the curl is contained within 13, 46, and 92 km of the coast, respectively. These profiles are somewhat arbitrary, but their scales reasonably represent differences between wind products (e.g., QuikSCAT and RSM [*Song et al.*, 2011]) and between different resolutions of the same wind product (e.g., COAMPS at 3, 9, and 27 km [*Capet et al.*, 2004]).

[8] The efficacy of upwelling for bringing deep water to the surface is measured by the source depth of upwelled waters. In past modeling studies, source water has been studied by tracking floats released at various depths [*Capet et al.*, 2004] or running passive tracers from the surface mixed layer (SML) backward in time with an adjoint model [*Chhak and Di Lorenzo*, 2007; *Song et al.*, 2011]. Here, we use a passive tracer in the forward model to answer the question: at any given time, what is the origin depth of water entering the SML from below? This calculation is accomplished as described in *Jacox and Edwards* [2011], by initializing the model with a "source depth tracer" that increases linearly with depth (see Figure 2). Flux of this tracer into the SML divided by volume transport into the SML gives a characteristic source tracer concentration, which is mapped directly to source depth. Though not all upwelling originates from this particular depth, it is a useful integrated measure for characterizing source waters.

3. Theory

[9] We investigate here the relative partitioning of total transport between the BBL and the interior, as this partitioning directly impacts the origin of flux into the SML. Because U^s, U^b, and U^i all vary with cross-shelf position, it is useful to define $U_i^b = U^b(x_i)$ and $U_o^s = U^s(x_o)$, where x_i is the position of the inner shelf boundary and x_o represents a position sufficiently far offshore that surface wind stress is approximately its asymptotic value. Further, we define $\mathcal{R}_u = \left|U_i^b / U_o^s\right|$ as the metric that captures the partitioning of BBL transport of interest. $\mathcal{R}_u$ represents the fraction of total upwelled transport deriving from the BBL (entering the SML through the inner shelf and not through the interior). By definition $1 - \mathcal{R}_u$ represents the remaining fraction, which derives from the ocean interior and enters the SML broadly over the region $x_o < x < x_i$ (Figure 1).

[10] *Lentz and Chapman* [2004, hereinafter LC04] developed a simple steady state upwelling theory and focused on the importance of cross-shelf momentum flux divergence, a commonly overlooked component of the vertically integrated alongshore momentum balance. In the eastern boundary upwelling configuration, alongshore velocity is assumed to be equatorward and to decay with depth. The alongshore momentum transported offshore in the SML is therefore greater than that transported onshore below the SML, resulting in a net offshore momentum flux (illustrated in Figure 2 of LC04). Since momentum flux across the coastal boundary is zero, there must also be a nonzero

divergence of cross-shelf momentum flux. LC04 showed the importance of this term in determining cross-shelf flow structure for spatially uniform winds in the absence of an alongshore pressure gradient. At high Burger numbers, cross-shelf momentum flux divergence balances surface stress, and onshore flow is relatively high in the water column. At low Burger numbers, surface wind stress is balanced primarily by bottom stress and onshore flow is concentrated in the BBL. Here, we repeat the LC04 derivation, with modifications where necessary to include cross-shelf variation in surface and bottom stresses. We first briefly present the calculations leading to equation (7), which are identical to those of LC04 except for a change of coordinate system. Beyond equation (7), the additional calculations and assumptions required of our theoretical extension are described.

[11] We assume geostrophic balance between the cross-shelf pressure gradient and the Coriolis force associated with alongshelf flow, and thermal wind balance between the cross-shelf density gradient and vertical shear in the alongshelf flow. Both of these assumptions are observationally supported, as outlined in LC04. Integration of the thermal wind balance from the surface to depth z, assuming $\partial\rho/\partial x$ is vertically uniform, yields

$$v(z) \approx v^s + \frac{g}{f\rho_0}\frac{\partial \rho}{\partial x} z, \tag{3}$$

where v^s is alongshelf surface velocity.

[12] As described in section 2, cross-shelf transport is divided into surface- and bottom-stress driven Ekman layers, and an interior component. In the 2D configuration, vertically integrated cross-shelf transport is zero and the vertical structure of cross-shelf velocity is described by

$$u^s = \frac{\tau^{sy}}{\rho_o f \delta^s}, \qquad -\delta^s < z < 0, \tag{4}$$

$$u^i = -\frac{\left(\tau^{sy} - \tau^{by}\right)}{\rho_o f h}, \qquad -h < z < 0, \tag{5}$$

$$u^b = -\frac{\tau^{by}}{\rho_o f \delta^b}, \qquad -h < z < -h + \delta^b, \tag{6}$$

where each component of cross-shelf velocity is assumed to be vertically uniform (LC04) and δ^s and δ^b are surface and bottom boundary layer thicknesses, respectively. Using $v(z)$ from equation (3) and $u(z)$ from equations (4)–(6), we vertically integrate the product to estimate cross-shelf momentum flux:

$$\int_{-h}^{0} uv\, dz \approx \frac{g}{2\rho_0 f}\frac{\partial \rho}{\partial x}\left[\frac{\tau^{sy}}{\rho_0 f}\left(\delta^s - h\right) + \frac{\tau^{by}}{\rho_0 f}\left(\delta^b - h\right)\right], \tag{7}$$

where τ^{sy} and τ^{by} are surface and bottom stresses, respectively, and h is bottom depth. From equation (7), LC04 quantify cross-shelf momentum flux divergence assuming no cross-shelf variations in δ^s, δ^b, τ^{sy}, τ^{by}, or $\partial\rho/\partial x$. Here, we rework their theory allowing the stresses to be functions of the cross-shelf coordinate, x. Note that while LC04 initially developed the theory for application farther offshore, it predicts modeled BBL transport quite well at the inner shelf boundary, though $\mathcal{R}_u$ is underestimated at higher Burger numbers ($S > 1$). Examination of momentum budgets in our model runs shows that the assumption of geostrophic balance for cross-shelf momentum is still reasonable near the inner shelf boundary (defined in practice here as the location where SML and BBL are separated by <10 m). Also, for simplicity we retain the assumption that δ^s and δ^b are independent of x, though this is clearly an oversimplification (see Figure 2, for example). However, numerical model results show that $\partial\delta^b/\partial x$ and $\partial\delta^s/\partial x$ are generally much smaller than $\partial h/\partial x$, making the omission of those terms reasonable. Following the derivation of LC04, which assumes that the isopycnal slope is proportional to water depth divided by the baroclinic deformation radius,

$$\frac{\partial\rho/\partial x}{\partial\rho/\partial z} \approx \pm a\frac{h}{Nh/f} = \pm a\frac{f}{N}, \tag{8}$$

we find

$$\frac{\partial}{\partial x}\int_{-h}^{0} uv\, dz \approx -b\frac{|\tau^{sy}|}{\rho_0}\frac{S}{2}\left(1 + \frac{\tau^{by}}{\tau^{sy}}\right) \pm b\frac{x}{\rho_0}\frac{S}{2}\left(\gamma^s\frac{\partial\tau^{sy}}{\partial x} + \gamma^b\frac{\partial\tau^{by}}{\partial x}\right), \tag{9}$$

where the plus and minus signs correspond to $\tau^{sy} < 0$ (upwelling for $f > 0$) and $\tau^{sy} > 0$ (downwelling for $f > 0$) conditions, respectively. Here, the proportionality constant a is replaced by b, which also accounts for differences in cross-shelf and alongshelf velocity profiles from their assumed vertical structure (LC04), and γ^s and γ^b represent the fraction of the water column not in the SML and BBL, respectively:

$$\gamma^s = \frac{h - \delta^s}{h} \qquad \text{and} \qquad \gamma^b = \frac{h - \delta^b}{h}. \tag{10}$$

Typically $\gamma^s \sim 0.5$ at the inner shelf boundary and approaches 1.0 offshore, even for constant boundary layer thickness δ^s. The analogous BBL term scales similarly. In the curl free case, equation (9) reduces to that derived by LC04; the second term is an adjustment due to surface and bottom stress curls. Under steady state conditions and assuming no alongshore pressure gradient, the vertically integrated alongshore momentum equation can be written,

$$\frac{\partial}{\partial x}\int_{-h}^{0} uv\, dz = \frac{\tau^{sy}}{\rho_0} - \frac{\tau^{by}}{\rho_0}, \tag{11}$$

into which equation (9) can be substituted. Under upwelling conditions ($\tau^{sy} < 0$) of central interest to this study, the bottom stress is then expressed

$$\tau^{by} = \tau^{sy}\frac{1 - bS/2}{1 + bS/2} - \frac{bS/2}{1 + bS/2}\left(\gamma^s x\frac{\partial\tau^{sy}}{\partial x} + \gamma^b x\frac{\partial\tau^{by}}{\partial x}\right). \tag{12}$$

Again, the first term on the right is equal to that derived by LC04, though τ^{sy} is uniform in their theory whereas here it is a function of x. The second term represents an adjustment

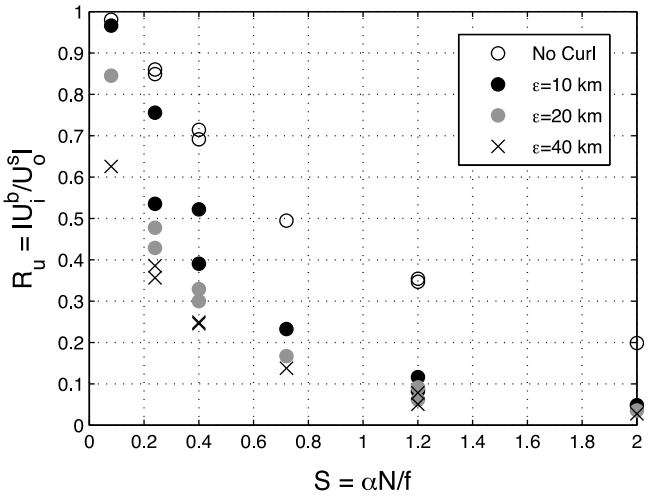

Figure 3. The relative contribution of bottom boundary layer transport to total upwelling transport after 10 days is shown as a function of Burger number. Markers indicate model results from four different surface forcings; the curl-free case and positive curl over three spatial scales.

due to local curl of surface and bottom stresses. For $f > 0$ and $\tau^{sy} < 0$, upwelling favorable conditions yield a negative bottom stress according to the first term. Positive wind and bottom stress curls result in a positive adjustment to this value according to the second term, because $x < 0$ within the domain. This reduction in bottom stress amplitude by the sum of stress curls indicates also an increase in the magnitude in the cross-shelf momentum flux divergence consistent with equation (11).

[13] Surface and bottom volume fluxes are given by Ekman transports associated with surface and bottom stresses, respectively. Far from shore, offshore surface transport in the curl case equals transport in the curl-free case,

$$U_o^s\big|_c = U_o^s\big|_{nc} = \frac{\tau_o^{sy}}{\rho_0 f} \qquad U_i^b = -\frac{\tau_i^{by}}{\rho_0 f}, \tag{13}$$

where subscripts c and nc indicate curl and no-curl cases, respectively, and subscripts o and i denote calculations at the offshore coordinate x_o and the inner shelf boundary x_i, respectively. From equations (12) and (13), the net change in relative transport $\mathcal{R}_u$ from the curl-free to the curl case is obtained:

$$\begin{aligned}\Delta\mathcal{R}_u &= \mathcal{R}_{u,c} - \mathcal{R}_{u,nc} \\ &= -\mathcal{R}_{u,nc}\left(1 - \frac{\tau_{c,i}^{sy}}{\tau_{nc}^{sy}}\right) - \frac{x_i}{\tau_{nc}^{sy}}\frac{bS/2}{1+bS/2}\left(\gamma^s\frac{\partial\tau_c^{sy}}{\partial x} + \gamma^b\frac{\partial\tau_c^{by}}{\partial x}\right)_i.\end{aligned} \tag{14}$$

The terms on the right hand side of equation (14) describe two theoretical means by which a nearshore drop-off in alongshore wind stress alters $\mathcal{R}_u$ relative to the curl-free case. The first is a reduction in BBL transport associated with reduced surface Ekman transport at the inner shelf boundary. In the curl case, surface wind stress at the inner shelf boundary is less than that in the curl-free case. BBL transport at the inner shelf boundary is therefore reduced, proportionate to the surface wind stress reduction at that location. The first term on the right hand side of equation (14) is less than zero, indicating that a smaller fraction of total upwelled water derives from the bottom boundary layer at the inner shelf boundary, and a greater fraction arrives from the interior. This term is greatest when wind stress at the inner shelf boundary is small compared to that offshore. The second term represents a curl-driven increase in the cross-shelf momentum flux divergence, and is greater for strong curl and high Burger numbers. Since $x < 0$ in the domain and $\tau_{nc}^{sy} < 0$ for upwelling, positive stress curls result in a further reduction in relative BBL transport.

[14] A major limitation of this theory, discussed further by LC04, is that there is no interaction between cross-shelf circulation and an evolving density field. Rather, the cross-shelf scale of sloping isopycnals is assumed to be the baroclinic deformation radius, and isopycnal slope is therefore proportional to f/N. It is valuable, therefore, to compare the theory to a numerical model with time-dependent dynamics. We present this comparison in the following section.

4. Results

[15] Variable structure in cross-shelf flow imparted by different wind patterns is clearly illustrated in the streamlines of Figure 2. Vertical transport in the curl-free case is strong, concentrated close to the coast, and largely contained in the BBL. Wind stress reduction nearshore results in horizontally distributed upwelling under the region of positive curl, and weaker vertical transport. These effects become more prominent as the horizontal scale of curl increases. As predicted by the theory in section 3, there is a shift in transport from the BBL to the interior associated with weakened winds nearshore, and several reasons for this are evident in Figure 2. The first is a reduction in surface Ekman transport (and associated BBL transport) in the region of curl, as described by equation (14). At a given offshore position x, surface Ekman transport is reduced as the cross-shelf scale of curl increases, and $U^b(x)$ drops accordingly. Furthermore, weaker nearshore wind stress reduces the offshore extent of the inner shelf, placing its boundary (where U_i^b is defined) at a position closer to shore and under even lower wind stress. Second, the structure of the BBL flow itself is visibly altered by wind stress curl. Although BBL volume transport is theoretically independent of x in the curl-free case, model simulations show BBL transport increasing monotonically with decreasing distance from shore as the BBL entrains water from the interior. While a similar entrainment occurs offshore under cyclonic wind stress curl forcing, streamlines exit the BBL just offshore of the inner shelf, and this fluid enters the SML from the interior.

[16] Surface and bottom boundary layer transports are calculated from the model as vertical integrals of zonal velocity between relevant limits. This practice technically includes non-Ekman (i.e., interior) transport that occurs within the boundary layers, but this contribution is generally small, and we neglect the difference between this value and the pure Ekman transport used in the theory. In general, $\mathcal{R}_u$ decreases at higher Burger numbers, and with increased scale of wind stress curl (Figure 3). However, the point at which a change in curl scale effects greatest change in $\mathcal{R}_u$ is dependent on slope and stratification. In the most weakly

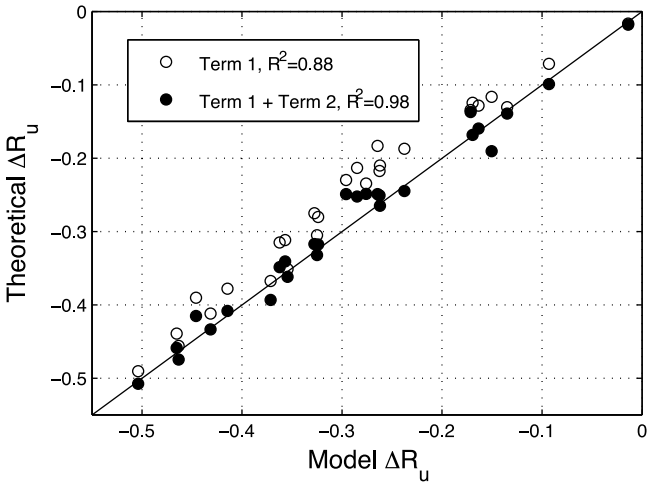

Figure 4. Change in $\mathcal{R}_u$ relative to the curl-free case is depicted for all 27 curl cases (runs 10–36 in Table 1), as measured in model simulations and predicted by theory. Terms 1 and 2 refer to the right-hand side of equation (14), with $b = 1$. Term 1 (Ekman transport adjustment) accounts for most of the shift in $\mathcal{R}_u$, and term 2 (cross-shelf momentum flux adjustment) improves model-theory agreement. Perfect agreement is indicated by solid line.

stratified, weakly sloping ($S = 0.08$) case, $\mathcal{R}_u$ changes little between the curl-free and $\epsilon = 10$ km cases, but substantially from $\epsilon = 10$ km to $\epsilon = 20$ km and from $\epsilon = 20$ km to $\epsilon = 40$ km. At high Burger numbers, effectively all the change occurs between the curl-free and $\epsilon = 10$ km cases, with little additional impact as ϵ is increased further. The key relationship here is between the cross-shelf scale of the curl and the position of the inner shelf boundary, where BBL transport enters the SML. In general, the inner shelf extends farther offshore with weaker stratification and reduced slope [*Jacox and Edwards*, 2011]. At our low Burger number extreme ($S = 0.08$), the inner shelf extends far (30–40 km) offshore and strong curl ($\epsilon = 10$ km) contained within that distance is effectively the same as no wind stress reduction in terms of transport partitioning. For $S = 2$, the inner shelf is confined extremely close to shore ($\lesssim$2 km), and curl over any of the three scales influences $\mathcal{R}_u$ similarly. In terms of fractional change in BBL transport, the greatest decrease is at high Burger numbers. While $\sim$25% of upwelling transport for $S = 2$ in the curl-free case is BBL derived, its contribution drops to $\sim$3% in the curl cases. As the BBL transport contribution to upwelling of deep waters is disproportionately high [*Jacox and Edwards*, 2011], this reduction in $|U_i^b|$ greatly reduces overall source depth.

[17] Figure 4 depicts the theoretical adjustment to BBL transport (equation (14)) as compared to numerical model results. Changes in Ekman transport at the inner shelf boundary (Term 1 in Figure 4) account for most of the transport partitioning adjustment, while the curl-driven change in cross-shelf momentum flux divergence (Term 2 in Figure 4) produces a smaller effect. Estimating the reduction in $\mathcal{R}_u$ by only the former process produces good model-theory agreement ($R^2 = 0.88$), which is further improved by including the latter effect ($R^2 = 0.98$). Contributions to Term 2 from wind stress curl and bottom stress curl are typically of similar scale. We note that bottom stress curl exists even in the curl-free wind stress case considered by LC04; however, its magnitude, and therefore its contribution to BBL transport, is generally small except at high Burger number.

[18] Though the theory presented here was developed for steady state, acceleration in the numerical model is significant even after 10 days, especially at high Burger numbers and farther offshore. Similarly, LC04 showed that at higher Burger numbers temporal acceleration contributes materially to the vertically integrated momentum budget,

$$\frac{\tau^{sy} - \tau^{by}}{\rho_0} = \frac{\partial}{\partial t}\int_{-h}^{0} v\,dz + \frac{\partial}{\partial x}\int_{-h}^{0} uv\,dz. \tag{15}$$

Their steady theory works well because, as they discuss, their estimate of the cross-shelf momentum flux divergence (with $b = 1$) overestimates that obtained numerically and partially accounts for temporal acceleration. In our numerical results we find that terms in the alongshelf momentum balance, when normalized by surface stress, are only slightly affected by wind stress curl. A small decrease in the amplitude of the bottom stress term is accompanied by modest adjustments of the integrals on the right hand side of equation (15). Therefore, changes to relative bottom stress are minor and are accurately predicted by equation (12).

[19] As stated previously, BBL transport draws from deeper than interior transport. It is not surprising therefore to see a general trend of increasing source depth with increasing $\mathcal{R}_u$ (Figure 5). Since $\mathcal{R}_u$ is dependent on Burger number (which includes shelf slope, stratification, and Coriolis frequency) as well as the scale of wind stress curl (Figure 3), all of these parameters also influence source depth. Increasing stratification or the scale of wind stress curl causes a decrease in $\mathcal{R}_u$ and, consequently, in upwelling source depth. However, the relationship between $\mathcal{R}_u$ and source depth is more complicated; for a given change in $\mathcal{R}_u$, the

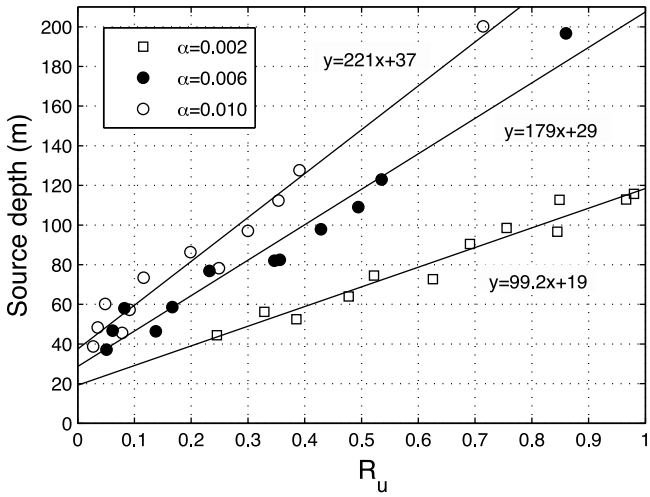

Figure 5. The relationship between $\mathcal{R}_u$ and mean upwelling source depth after 10 days is depicted for all 36 model runs. Model configurations with different shelf slope, α, are indicated by different marker types (each marker type includes 3 different stratifications and 4 different wind patterns), and linear fits are shown for each shelf slope.

change in source depth is greater with steeper shelf slope. For example, our results show that for $\Delta\mathcal{R}_u = 0.1$, source depth increases by 9.9, 17.9, and 22.1 m for α = 0.002, 0.006, and 0.010, respectively. As described in *Jacox and Edwards* [2011], water of a given depth is laterally closer to shore in steep slope cases, and reaches the inner shelf faster with the same horizontal velocity. As $\mathcal{R}_u$ decreases (high Burger number, weak nearshore winds), source depth decreases to a projected minimum of 20–40 m on day 10 in the case of no BBL transport. At the other extreme, where all transport derives from the BBL, source depths on day 10 reach 120–260 m, depending on shelf slope.

5. Discussion

[20] Through the suite of numerical model runs performed here, we investigated the effects of slope, stratification, and wind stress curl on upwelling source depth and partitioning of vertical transport. Ranges of slope and stratification were chosen to cover those seen in major global upwelling regions, and wind stress curl was varied over a range of scales that could be representative of spatial or temporal variability, different wind products, or different resolutions of the same wind product. We find that as the cross-shelf scale of curl increases, upwelling transport increasingly derives from the interior rather than the BBL, with the greatest fractional reduction in $\mathcal{R}_u$ at high Burger numbers. Mean upwelling source depth increases linearly with $\mathcal{R}_u$ for a given shelf slope, and increases more rapidly with $\mathcal{R}_u$ over steeper slopes.

[21] We find that evaluating the impact of nearshore curl on upwelling source depth requires consideration of not just the scale of the curl, but also the width of the inner shelf. Weak stratification and gradual shelf slope produce a wider inner shelf than strong stratification and steep slope, and consequently different scales at which changes in curl are most important. Reduction of $\mathcal{R}_u$ due to a nearshore wind stress drop-off is minimal if the drop-off occurs primarily over the inner shelf, and substantial if it occurs offshore of the inner shelf boundary. A third cross-shelf scale, the one over which coastal upwelling occurs, may be important for distinguishing the coastal and curl-driven upwelling components. Classifying coastal divergence as only the transport driven by the coastal wind stress would underestimate its contribution; upwelling associated with the mean wind stress over the width of the coastal upwelling zone may be a more accurate measure. However, we do not attempt to separate these components while exploring the impacts of nearshore curl on upwelling dynamics, and in fact they are not independent. In the nearshore curl region, Ekman pumping raises isopycnals in the interior of the water column, altering source waters for coastal upwelling and likely increasing resultant nutrient fluxes.

[22] By definition, the separation of U^b and U^i distinguishes flux to the inner shelf from that supplying the mid and outer shelf, offshore of the upwelling front. These regions are likely to support different biological communities, with larger plankton sustained by strong upwelling and substantial nutrient flux nearshore and smaller plankton supported by weaker offshore upwelling [*Rykaczewski and Checkley*, 2008]. Our results therefore suggest that the retentive inner shelf region, supporting larger plankton, should be wide and productive in the presence of weak stratification and wind stress that remains strong close to shore. Strong stratification and substantial nearshore wind stress reduction, on the other hand, should support smaller plankton in a large region of cyclonic wind stress curl. The effect of shelf slope is less clear in this regard due to a tradeoff between conditions favorable to growth of large plankton. Weaker slopes promote BBL transport and produce a wider inner shelf, but steeper slopes allow upwelling of deeper water, presumably richer in nutrients.

[23] Questions regarding the relative importance of curl-driven and coastal upwelling have persisted in the literature for at least a decade, generally in the form; (1) How does the reduction in nearshore wind stress (i.e., cyclonic curl) affect upwelling transport? and (2) How do changes in this structure alter the source waters for upwelling? However, modeling studies designed to address these questions have been performed in different regions, with different wind products, and using different metrics to quantify upwelling. For example, *Capet et al.* [2004] investigated a CCS model, used QuikSCAT winds for the "weak curl" case, released floats to quantify upwelling, and found that cyclonic curl does not compensate for reduced coastal wind stress. *Albert et al.* [2010] investigated the Peru current system, used QuikSCAT winds for the "strong curl" case, evaluated the efficacy of upwelling with nutrient and chlorophyll diagnostics from a biogeochemical model, and found decreased coastal divergence to be overcompensated by curl-driven upwelling. Though these studies and others seem to offer contrary conclusions on the relative importance of coastal and curl-driven upwelling, we believe their findings, in light of the present study, can be reconciled when differences in methods and upwelling metrics are considered. In general: (1) total upwelling transport is determined primarily by wind stress far offshore ($|x| \gg \epsilon$) rather than the curl structure, though the relative contribution of coastal divergence decreases as nearshore wind stress decreases, and (2) upwelling source depth is altered by the cross-shelf wind profile, and increases as high offshore winds extend closer to the coast. However, there are complex interactions between wind stress, stratification, and topography that exert important influence on upwelling dynamics (Figure 3) and make direct comparison between studies difficult. In addition, important dynamics not captured in the present study should be considered, including (1) though nutrients in the ocean typically increase with depth, nutrient fluxes are not necessarily coupled to source depth in EBCs, where decreased source depth may accompany a curl-driven shoaling of the nutrient-rich poleward undercurrent, (2) *Fennel and Lass* [2007] argued that decreased Ekman transport can actually be overcompensated by Ekman pumping due to inhibition of coastal upwelling by coastally trapped waves, and (3) the ability of an alongshore pressure gradient to modify upwelling dynamics has been well documented, and is not included in our 2D model.

[24] **Acknowledgments.** We gratefully acknowledge funding from the Gordon and Betty Moore Foundation and National Science Foundation grant OCE0726858. Comments from two anonymous reviewers greatly improved the manuscript. We also thank Jenny Quay for many helpful discussions.

References

Albert, A., V. Echevin, M. Lévy, and O. Aumont (2010), Impact of nearshore wind stress curl on coastal circulation and primary productivity in the Peru upwelling system, *J. Geophys. Res.*, *115*, C12033, doi:10.1029/2010JC006569.

Capet, X. J., P. Marchesiello, and J. C. McWilliams (2004), Upwelling response to coastal wind profiles, *Geophys. Res. Lett.*, *31*, L13311, doi:10.1029/2004GL020123.

Chhak, K., and E. Di Lorenzo (2007), Decadal variations in the California Current upwelling cells, *Geophys. Res. Lett.*, *34*, L14604, doi:10.1029/2007GL030203.

Croquette, M., G. Eldin, C. Grados, and M. Tamayo (2007), On differences in satellite wind products and their effects in estimating coastal upwelling processes in the south-east Pacific, *Geophys. Res. Lett.*, *34*, L11608, doi:10.1029/2006GL027538.

Dever, E. P., C. E. Dorman, and J. L. Largier (2006), Surface boundary-layer variability off Northern California, USA, during upwelling, *Deep Sea Res., Part II*, *53*, 2887–2905.

Enriquez, A. G., and C. Friehe (1995), Effects of wind stress and wind stress curl variability on coastal upwelling, *J. Phys. Oceanogr.*, *25*, 1651–1671.

Fennel, W., and H. U. Lass (2007), On the impact of wind curls on coastal currents, *J. Mar. Syst.*, *68*, 128–142.

Jacox, M. G., and C. A. Edwards (2011), Effects of stratification and shelf slope on nutrient supply in coastal upwelling regions, *J. Geophys. Res.*, *116*, C03019, doi:10.1029/2010JC006547.

Koracin, D., C. E. Dorman, and E. P. Dever (2004), Coastal perturbations of marine layer winds, wind stress, and wind stress curl along California and Baja California in June 1999, *J. Phys. Oceanogr.*, *34*, 1152–1173.

Lentz, S. J., and D. C. Chapman (2004), The importance of non-linear cross-shelf momentum flux during wind-driven coastal upwelling, *J. Phys. Oceanogr.*, *34*, 2444–2457.

Messié, M., J. Ledesma, D. D. Kolber, R. P. Michisaki, D. G. Foley, and F. P. Chavez (2009), Potential new production estimates in four eastern boundary upwelling ecosystems, *Prog. Oceanogr.*, *83*, 151–158, doi:10.1016/j.pocean.2009.07.018.

Pickett, M. H., and J. D. Paduan (2003), Ekman transport and pumping in the California Current based on the U.S. Navy's high-resolution atmospheric model (COAMPS), *J. Geophys. Res.*, *108*(C10), 3327, doi:10.1029/2003JC001902.

Rykaczewski, R. R., and D. M. Checkley (2008), Influence of ocean winds on the pelagic ecosystem in upwelling regions, *Proc. Natl. Acad. Sci.*, *105*, 1965–1970.

Shchepetkin, A. F., and J. C. McWilliams (2005), The Regional Ocean Modeling System: A split-explicit, free-surface, topography following coordinates ocean model, *Ocean Modell.*, *9*, 347–404.

Song, H., A. J. Miller, B. D. Cornuelle, and E. Di Lorenzo (2011), Changes in upwelling and its water sources in the California Current System driven by different wind forcing, *Dyn. Atmos. Oceans*, *52*, 170–191.